Nanoscale

Accepted Manuscript

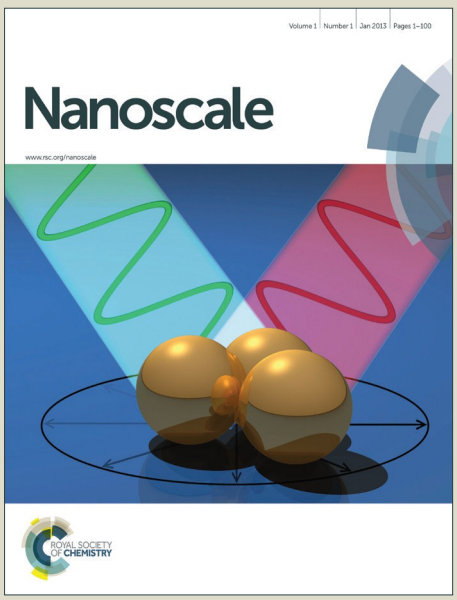

ROYAL SOCIETY OF CHEMISTRY

www.rsc.org/nanoscale

Nanoscale

PAPER

$CoPt/CeO_2$ Catalysts for Growth of Narrow Diameter Semiconducting Single-walled Carbon Nanotubes

Received 00th January 20xx,
Accepted 00th January 20xx

DOI: 10.1039/x0xx00000x

www.rsc.org/

Lei Tang,[a,b] Taotao Li,[a] Chaowei Li,[a,b] Lin Ling,[a] Kai Zhang,[a] Yagang Yao*[a]

For the application of single-walled carbon nanotubes (SWNTs) in nanoelectronic devices, effective techniques for the growth of semiconducting SWNTs (s-SWNTs) with specific diameter are still a great challenge. Herein, we report a facile strategy for selective growth of narrow diameter distributed s-SWNTs by using $CoPt/CeO_2$ catalysts. The addition of Pt into Co catalyst dramatically reduces the diameter distributions and even the chirality distributions of the as-grown SWNTs. Oxygen vacancies that are provided by mesoporous CeO_2 is responsible for creating oxidative environment to in situ etch metallic SWNTs (m-SWNTs). Atomic force microscope (AFM) and Raman spectroscopy characterizations indicate the narrow diameter distribution of 1.32 ± 0.03 nm and the selectively growth of s-SWNTs to 93%, respectively. In addition, electronic transport measurements also confirm the I_{on}/I_{off} ratio mainly presents of ~10^3. This work provides an effective strategy for facile fabrication of narrow diameter distributed s-SWNTs, which will be beneficial to fundamental researches and broad applications of SWNTs for future nanoelectronics.

Introduction

Single-walled carbon nanotubes (SWNTs) have been the star material in the field of nanomaterial and nanotechnology due to their special structures and extraordinary properties since they were discovered.[1-4] Especially in the nanoelectronic devices, SWNTs have been regarded as one of the best candidates for channel materials in various transistors.[5-12] However, the coexistence issue of semiconducting SWNTs (s-SWNTs) and metallic SWNTs (m-SWNTs) heavily decreased the performance of their nanoeletronic devices. Up to date, direct chemical vapor deposition (CVD) growth[13-22] and CNTs separation methods[23, 24] have been developed for the preparation of s-SWNTs. Compared with the time-consuming and costly separation process, the direct CVD growth is considered to be a better way for the production of s-SWNTs, which is usually based on a proper oxidative environment for effectively in situ etching of m-SWNTs and the resulting s-SWNTs can reach over 90%. Moreover, in order to satisfy the need of SWNTs-based highly integrated circuits, homogeneous structural parameters of s-SWNTs, especially their uniform diameter and eventually chirality, are very desirable to the stability and reliability of highly integrated circuits.[25, 26] Accordingly, it is significant to explore a facile technique for the selective growth of narrow diameter distributed s-SWNTs.

Generally, both theoretical calculation[27, 28] and experimental studies[29-33] have demonstrated that the catalysts play an important role in controlling the diameter of SWNTs in the direct CVD growth process. Several research groups attempt to control the catalysts to realize the narrow diameter distribution of SWNTs, but such strategies are unable to distinguish s-SWNTs from metallic types, which heavily restricts the performance of nanoeletronic devices.

Herein, a facile and effective synthesis strategy was developed to selectively grow s-SWNTs with a narrow diameter distribution. In our typical atmospheric pressure chemical vapor deposition (APCVD) growth method, we chose CoPt bimetallics as the catalysts because the addition of Pt into a Co catalyst could dramatically reduce the diameter distributions of the catalysts and even the chirality distributions of the as-grown SWNTs. Considering the agglomerations of catalysts in CVD growth process, we utilized the mesoporous CeO_2 as the supports due to their high surface areas and uniform pore distribution features, which could help avoid agglomerations of catalyst nanoparticles at high growth temperature.[34] On the other hand, the cerium (IV) oxide could provide the proper oxidative environment for in situ etching m-SWNTs during SWNTs growth process by releasing oxygen vacancies. It has been demonstrated that the cerium (IV) oxide could transform into cerium (III) oxide.[35] There is no doubt that this special ability of releasing oxygen vacancies in CeO_2 could make a remarkable oxidative environment for in situ etching m-SWNTs.[36] Thus, $CoPt/CeO_2$ catalysts were used in this study. AFM and Raman characterizations indicated the narrow diameter distribution of 1.32 ± 0.03 nm and the selectively growth of s-SWNTs to 93%, respectively. In addition, electronic transport measurements show the high I_{on}/I_{off} ratio of ~10^3, confirming the formation of s-SWNTs.

[a] Division of Advanced Nanomaterials, Key Laboratory of Nanodevices and Applications, Suzhou Institute of Nano-tech and Nano-bionics, Chinese Academy of Sciences, University of Chinese Academy of Sciences, Suzhou 215123, China. E-mail: ygyao2013@sinano.ac.cn
[b] School of Sciences, Shanghai University, Shanghai 200444, China.
† Electronic Supplementary Information (ESI) available:
See DOI: 10.1039/x0xx00000x

This work provides an effective strategy for facile fabrication of narrow diameter distribution s-SWNTs, which would be beneficial to fundamental researches and broad applications of SWNTs for future nanoelectronics.

Experimental Section

Synthesis of mesoporous CeO_2 by hydrothermal method: 1.0 g of $Ce(NO_3)_3{\cdot}6H_2O$ was dissolved in 1 mL of deionized water. After that, 1 mL of CH_3COOH and 30 mL of glycol were added with stirring to form a uniform solution. The mixed solution was sealed and heated at 180 °C for 200 min to get the products.

Synthesis the CoPt/CeO_2 catalyst precursors by impregnation method: 0.021 g $Co(Ac)_2{\cdot}4H_2O$ was firstly added into 10 mL ethanol and sonicated for 15 min. Then, 220 μL $H_2PtCl_6{\cdot}6H_2O$ ethanol solution (0.05 mol/L) was added into the above solution and the mixture were sonicated for another 15 min. After that, 0.05 g CeO_2 were added to make the CeO_2 supported CoPt bimetallic catalysts with Co:Pt mole ratio of 1:1. Then, they were further sonicated for 1 h and baked at 80 °C for 12 h to evaporate the ethanol solution. After grinding in a mortar for 15 min to obtain fine powders, they were dispersed into ethanol solution again to obtain the supernatant for the subsequent catalysts.[37]

Synthesis the Co/CeO_2 catalyst precursors by impregnation method: 0.021 g $Co(Ac)_2{\cdot}4H_2O$ was firstly added into 10 mL ethanol and sonicated for 15 min. Then, 0.05 g CeO_2 were added to make the CeO_2 supported Co catalysts. Then, they were further sonicated for 1 h and baked at 80 °C for 12 h to evaporate the ethanol solution. After grinding in a mortar for 15 min to obtain fine powders, they were dispersed into ethanol solution again to obtain the supernatant for the subsequent catalysts.

Growth of SWNTs on SiO_2/Si substrates: The SiO_2/Si wafer with a layer of 500 nm SiO_2 (purchased from Hefei Kejing Materials Technology Co., China) was used as substrates. Cleaning with deionized water (18.2 MΩ), acetone (AR), ethanol (AR) and deionized water for 15 min one by one, further needing to be blown dry with argon. Then 0.05 mmol/L CoPt/CeO_2 catalyst precursors ethanol solution were dispersed onto the substrates by the spin-coating method (2500 r/min, 1 min). The general CVD growth was conducted under atmospheric pressure in 1 inch quartz tube which was heated by a horizontal tube furnace (TF55035C-1 Lindberg/ Blue M). The SiO_2/Si substrates with well-dispersed catalyst species were put into the tube and heated in air to the expected temperature. Briefly, after sintering at 850 °C for 30 min in air, the system was purged with 300 sccm (standard cubic centimeter per minute) argon, and then 50 sccm hydrogen and 30 sccm argon (through an ethanol bubbler) were introduced for the growth of SWNTs at 850 °C for 20 min.

Fabrication and measurements of FETs devices: Back-gated FETs device with channel length of 2 μm and width of 30 μm were patterned by e-beam lithography (EBL) method firstly. Then the 50 nm Pd was deposited by e-beam evaporation (EBE) as the contact metal. Surrounding carbon nanotubes of the FETs devices were etched by a reactive ion etching (RIE, oxygen) system to prevent electric leakage during the measurements. Finally the source and drain electrodes were deposited with Ti (5 nm)/Au (50 nm) composite structrue.

Characterizations: The as-grown SWNTs were analyzed with the scanning electron microscopy (SEM, Hitachi S4800 field emission (1 kV)), atomic force microscopy (AFM, Veeco NanoScope IIIA,Veeco Co.), and Raman spectroscopy (Horiba HR800 Raman system). X-ray diffraction (XRD, Bruker AXS D8 Advance X-ray diffractometer with a Cu Ka radiation target (40 V, 40 A)) and transmission electron microscope (TEM, JEOL ARM 200F (200 kV)) and N_2 adsorption/desorption (3H-2000BET-A) were used to characterize the as-prepared mesoporous CeO_2. X-ray photoelectronic spectroscopy (XPS, ESCALab250, Thermo Scientific Corporation) was used to confirm the chemical composition of CoPt bimetallic catalysts and to verify oxygen vacancies in mesoporus CeO_2. Transmission electron microscope (TEM, JEOL ARM 200F (200 kV)) was applied to characterize the microscopic structure of the CoPt bimetallic catalysts, and optical microscope was utilized to characterize the as-fabricated FETs device. The electrical measurement was performed by a Keithley 4200-SCS semciconductor characterization system. The source-drain voltage was 100 mV.

Results and discussion

Figure 1a schematically illustrates the process of selective growth of narrow diameter distributed s-SWNTs using CoPt/CeO_2 catalysts. The CoPt/CeO_2 catalysts were synthesized by impregnation method using $Co(Ac)_2{\cdot}4H_2O$ and $H_2PtCl_6{\cdot}6H_2O$ ethanol solution as catalyst precursors, mesoporous CeO_2 as the catalyst supports. After sonication and impregnation for hours, CoPt/CeO_2 catalysts were dispersed onto the substrates, and then underwent oxidation and sintering at 850 °C for 30 min in open-end quartz tube. The growth was conducted in the general CVD system. After purging with 300 sccm argon, 50 sccm hydrogen and 30 sccm argon (through an ethanol bubbler) were introduced for the growth of SWNTs at 850 °C for 20 min. Mesoporous CeO_2 was chosen because it can serve as the support to prevent the bimetallic catalysts from agglomerations, and also to provide oxygen vacancies, which is believed to inhibit the formation of m-SWNTs. m-SWNTs can be easily etched away under oxidative environment during CVD process because of their special electronic structure. Mesoporous CeO_2 was prepared by hydrothermal method. As-prepared CeO_2 was confirmed by XRD shown in **Figure S1**. The microscopic structure of CeO_2 was acquired from TEM as shown in **Figure S2**, which indicates an uniform size with a narrow size distributions. Further characterization shows that the CeO_2 has high surface areas (**Figure S3a**, S_{BET} = 224.78 m^2/g, $S_{Brunauer\text{-}Emmet\text{-}Teller}$) and displays a mesoporous type of IV N_2 adsorption/desorption isotherm as well as uniform pore distribution of 6.0 ± 0.3 nm (**Figure S3b**).

Figure 1b shows a typical SEM image of as-grown SWNTs. Higher magnification SEM image in **Figure 1c** and AFM image in **Figure 1d** show the as-grown SWNTs have uniform length, which would be suitable for various transistors as channel materials. **Figure 1e** is the diameter histogram of as-grown SWNTs, which shows a narrow distribution of 1.32 ± 0.03 nm with Gauss linear fitting

analysis pattern. Raman spectroscopy was used to characterize the conduction type of SWNTs based on their radial breathing mode (RBM) band frequencies and the excitation wavelength.[38, 39] According to the Kataura Plot,[40] under 532 nm excitation laser, the expected Raman shift frequency of RBMs between 100−119 and 207−275 cm^{-1} are regarded to be m-SWNTs while SWNTs with RBMs from 119 to 207 cm^{-1} are s-SWNTs. Under 633 nm excitation laser, SWNTs with RBMs from 177 to 221 cm^{-1} are considered to be m-SWNTs, and the other RBMs ranging from 100 to 275 cm^{-1} belong to s-SWNTs. **Figure 1f** and **1g** show typical RBM peaks for the as-grown SWNTs with 532 nm and 633 nm wavelength excitation, respectively. It is clearly indicated that s-SWNT peaks are the overwhelming majority, while m-SWNTs peaks are barely present. From **Figure S4**, the as-grown SWNTs obviously show typical s-SWNTs peak features. Tangential vibration (G mode) bands at 1580 cm^{-1} does not exhibit the Breit−Wigner−Fano (BWF) line shape, which is a typical feature of m-SWNTs.[40] In addition, from the low D/G ratio in **Figure S5**, we can know that the as-grown SWNTs take on excellent quality, which may be attributed to oxygen vacancies in CeO_2 providing the oxidative environment for etching amorphous carbon during the general CVD process. **Figure S6** shows typical TEM image of as-grown SWNTs. To further verify that oxygen vacancies in CeO_2 play a key role for in situ etching of m-SWNTs, control experiments were conducted by utilizing CoPt bimetallic catalysts without CeO_2 supports for SWNTs growth in the same condition. **Figure 7Sa** and **7Sb** show SEM images of SWNTs grown by CoPt catalysts, which display no obvious difference from the SEM images of SWNTs by CoPt/CeO_2 in **Figure 1b** and **1c**. However, Raman results in shown **Figure 7Sc** and **7Sd** demonstrate that the as-grown SWNTs do not have the metallic and semiconducting selectivity.

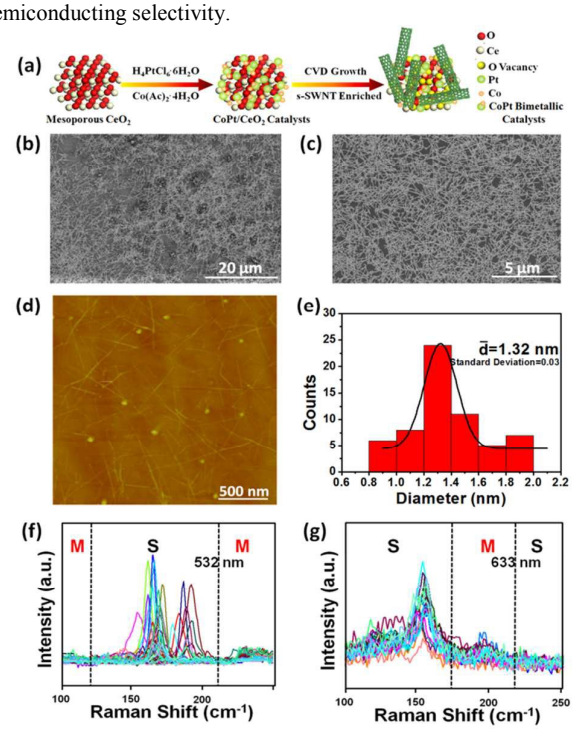

Figure 1. (a) Schematic illustration of selective growth of s-SWNTs by CoPt/CeO_2 catalysts; (b) and (c) SEM images of as-grown SWNTs using CoPt/CeO_2 catalysts; (d) Typical AFM image of as-grown SWNTs; (e) The corresponding diameter distribution of the SWNTs; (f) and (g) RBM peaks for the as-grown SWNTs samples with 532 nm and 633 nm wavelength excitation, respectively. Peaks within the dashed zones marked with S corresponded to the s-SWNTs, and M denoted the m-SWNTs.

We also used Co/CeO_2 as catalysts to confirm the role of Pt. As we all know, Co has high dissolution as well as adsorption of carbon, which may lead to wide diameter distribution and poor s-SWNTs selectivity. **Figure 2a** and **2b** show typical SEM iamges of the as-grown SWNTs using Co/CeO_2 catalysts. AFM and Raman spectroscopy characterizations indicate the broad diameter distribution (**Figure 2c** and **2d**) and the unfavorable semiconducting selectivity (**Figure 2e** and **2f,** 85% s-SWNTs), respectively.

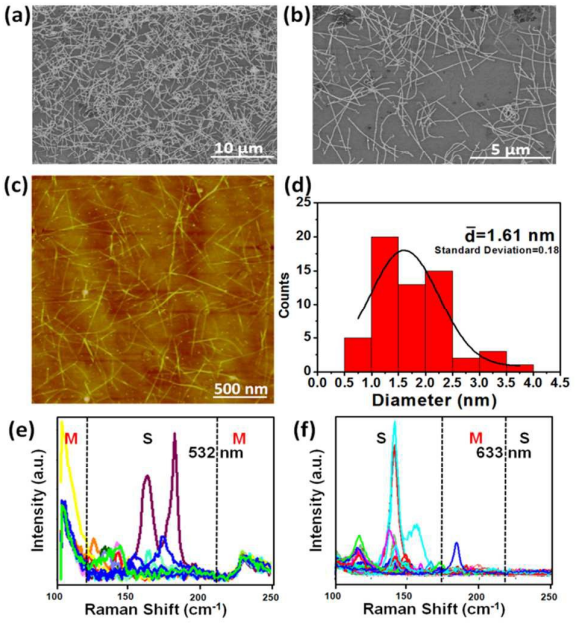

Figure 2. (a) and (b) SEM images of the SWNTs using Co/CeO_2 catalysts; (c) Typical AFM image of SWNTs using Co/CeO_2 catalysts; (d) The corresponding diameter distribution of the as-grown SWNTs; (e) and (f) RBM peaks for the as-grown SWNTs samples with 532 nm and 633 nm wavelength excitation, respectively. Peaks within the dashed zones marked with S corresponded to s-SWNTs, and M denoted m-SWNTs. The selectively growth of s-SWNTs is 85%.

The role of Pt in the SWNTs growth process was indirectly testified by TEM characterization of CoPt/CeO_2 which underwent serious of high temperature treatment. As shown in **Figure S8a** the catalysts are well-dispersed with narrow diameter distribution, which is suitable for the growth of narrow diameter distributed SWNTs. The background in **Figure S8a** is partial section of the CeO_2 support, and the full image of CeO_2 support is displayed in **Figure S2**. **Figure S8b** is the histogram of the diameter for the CoPt bimetallic catalysts size and shows average size of 2.94 nm. The component of the CoPt bimetallic catalysts were analyzed by XPS based on the valence state of the CoPt nanoparticles. In XPS analysis, **Figure 3a** shows the XPS spectra of the Pt in the CoPt nanoparticles. Double

peaks with the binding energy of Pt $4f_{7/2}$ peak at 71.80 eV and Pt $4f_{5/2}$ peak at 75.00 eV are observed, shifting from the standard value of pure Pt $4f_{7/2}$ peak at 71.20 and Pt $4f_{5/2}$ peak at 74.53 eV. **Figure 3b** shows that Co $2p_{3/2}$ peak at 779.00 eV and Co $2p_{1/2}$ peak at 794.30 eV slightly shift from the standard value of pure Co $2p_{3/2}$ peak at 778.30 eV, Co $2p_{1/2}$ peak at 793.27 eV. These shifts of both Co and Pt are consistent with the fact that Co alloys with Pt in the process.[41, 42] From XPS studies, we can see that that fine interation existes between as-reduced Pt and as-reduced Co in the CoPt bimetallics.

To verify oxygen vacancies in mesoporus CeO_2 at high temperature playing an important role for inhibiting the formation of m-SWNTs, we utilized XPS to investigate the states of catalyst supports before and after SWNTs growth. One sample was treated in a one inch quartz tube furnace at 850 °C for 30 min in air. Another sample was annealed in air at 850 °C for 30 min, then in a flow of 300 sccm argon and 30 sccm hydrogen for 20 min, and finally under the argon and hydrogen to cool down to room temperature. **Figure 3c** and **3d** show the full XPS spectra of CeO_2 and peaks in the Ce 3d region before SWNTs growth, respectively. **Figure 3e** and **3f** show the full XPS spectra of CeO_2 and peaks in the Ce 3d region after SWNTs growth, respectively. Utilizing the ratio of peak areas in XPS spectra corresponding to Ce^{3+} and Ce^{4+} before and after SWNTs growth, we find that the ratio of Ce^{3+}/Ce^{4+} changed from 5/10 to 12/10 after the SWNTs growth, indicating that the introduction of hydrogen at high growth temperature could reduce cerium (IV) oxide back into cerium (III) oxide, which might lead to the shift of some oxygen atoms to yield oxygen vacancies. The ability of releasing oxygen vacancies in CeO_2 provides a remarkable oxidative environment for in situ etching m-SWNTs during the CVD process.

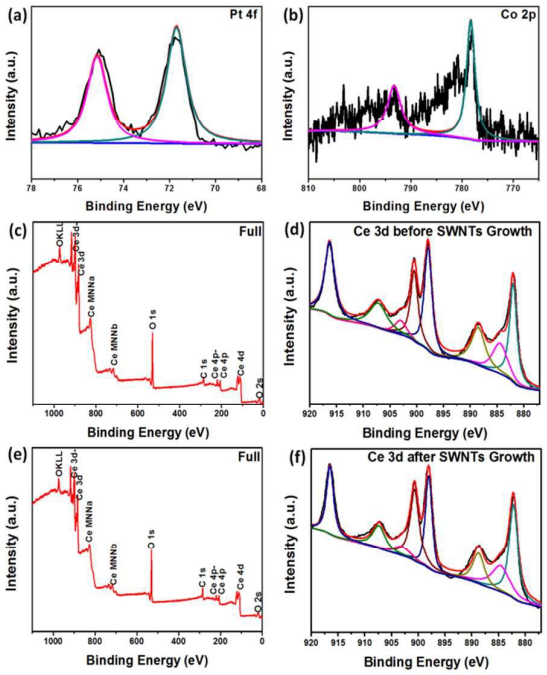

Figure 3. (a) XPS for the peak in the Pt 4f region; (b) XPS for the peak in the Co 2P region; The full spectra of XPS (c, e) and the peak in the Ce 3d region (d, f) of obtained CeO_2 before (c, d) and after (e, f) SWNTs growth.

Finally，to further prove the selective growth of s-SWNTs, we carried out the electrical measurements in the back gated field effect transistors (FETs) with as-grown SWNTs using $CoPt/CeO_2$ catalysts. The FET devices underwent sequent fabrications and test processes. **Figure 4a** and **4b** show the schematic illustration and the SEM image of a representative FET device. **Figure S9** shows the typical optical microscope image of the as-fabricated FET device. The FET device was fabricated on the as-grown SWNTs on SiO_2/Si substrate with 500 nm SiO_2 dielectrics. The channel length and width were 2 μm and 30 μm, respectively.[15, 43] Highly doped Si was used as the back gate, and the source-drain voltage was 100 mV. **Figure 4c** provides a typical I_{ds}-V_g transfer characteristic curve of as-fabricated device with V_{ds}=100 mV. The current on/off ratio is of ~367, which reveals typical semiconducting behavior of the channel materials. **Figure 4d** is the histogram of the I_{on}/I_{off} ratio for each device, and the current on/off ratio mainly presents of $\sim 10^3$. The results of electrical measurements are consistent with the obtained results by Raman measurement. We also carried out the electrical measurements in the back gated field effect transistors (FETs) with as-grown SWNTs using CoPt catalysts underwent the same process as described above. **Figure S10a** show the typical I_{ds}-V_g transfer characteristic curve of as-fabricated device with V_{ds}=100 mV, and the current on/off ratio is of ~3.1. **Figure S10b** is the histogram of the I_{on}/I_{off} ratio for as-fabricated devices using as-grown SWNTs using CoPt catalysts, and the current on/off ratio mainly presents of ~10. From the above results, we can conclude that we have successfully achieved the selective growth of narrow diameter distributed s-SWNTs utilizing $CoPt/CeO_2$ catalysts.

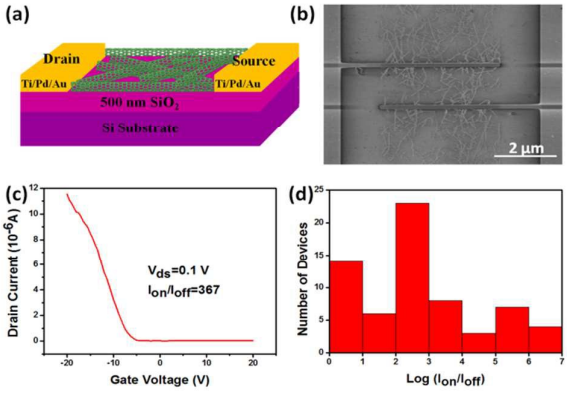

Figure 4. (a) Schematic illustration of the SWNTs FETs device; (b) SEM image of FETs device fabricated on the as-grown SWNTs on SiO_2/Si substrate with a channel length of 2 μm; (c) A typical transfer characteristic curve of as-fabricated device with V_{ds}=100 mV; (d) Histogram of the I_{on}/I_{off} ratio for each device.

Conclusions

In summary, we have developed a facile and effective approach to realize selective growth of narrow diameter distributed s-SWNTs based on synergistic utilization of $CoPt/CeO_2$ catalysts. As a result, we obtained s-SWNT with narrow-diameter distribution of 1.32 ± 0.03 nm on SiO_2/Si substrate. The s-SWNTs were confirmed by Raman spectroscopy and electronic transport measurements. Raman

characterizations indicated the selectively growth of s-SWNTs to 93%. In addition, electronic transport measurements show the high I_{on}/I_{off} ratio of ~10^3, confirming the formation of s-SWNTs. XPS spectra revealed that oxygen vacancies in mesoporous CeO_2 played an important role for the selectively preferential growth of s-SWNTs. This synergistic strategy offers more possibiliies for the structure controlled growth of SWNTs.

Acknowledgements

This work was supported by Natural National Science Foundation of China (No.51372265), and the Natural Science Foundation of Jiangsu Province, China (No. BK20140392).

Notes and references

1 S. Iijima and T. Ichihashi, *Nature*, 1993, **363**, 603.
2 R. H. Baughman, A. A. Zakhidov and W. A. de Heer, *Science*, 2002, **297**, 787.
3 C. Rutherglen, D. Jain and P. Burke, *Nat. Nanotechnol*., 2009, **4**, 811.
4 M. F. De Volder, S. H. Tawfick, R. H. Baughman and A. J. Hart, *Science*, 2013, **339**, 535.
5 M. Bockrath, D. H. Cobden, P. L. McEuen, N. G. Chopra, A. Zettl, A. Thess and R. E. Smalley, *Science*, 1997, **275**, 1922.
6 S. J. Tans, A. R. Verschueren and C. Dekker, *Nature*, 1998, **393**, 49.
7 A. Javey, H. Kim, M. Brink, Q. Wang, A. Ural, J. Guo, P. McIntyre, P. McEuen, M. Lundstrom and H. Dai, *Nat. Mater*, 2002, **1**, 241.
8 A. Javey, J. Guo, Q. Wang, M. Lundstrom and H. Dai, *Nature*, 2003, **424**, 654.
9 C. Wang, J. Zhang, K. Ryu, A. Badmaev, L. G. De Arco and C. Zhou, *Nano Lett*., 2009, **9**, 4285.
10 V. Derenskyi, W. Gomulya, J. M. S. Rios, M. Fritsch, N. Fröhlich, S. Jung, S. Allard, S. Z. Bisri, P. Gordiichuk and A. Herrmann, *Adv.Mater.*, 2014, **26**, 5969.
11 M. M. Shulaker, G. Hills, N. Patil, H. Wei, H.-Y. Chen, H.-S. P. Wong and S. Mitra, *Nature*, 2013, **501**, 526.
12 A. D. Franklin, *Nature*, 2013, **498**, 443.
13 Y. Li, D. Mann, M. Rolandi, W. Kim, A. Ural, S. Hung, A. Javey, J. Cao, D. Wang and E. Yenilmez, *Nano Lett.*, 2004, **4**, 317.
14 L. Ding, A. Tselev, J. Wang, D. Yuan, H. Chu, T. P. McNicholas, Y. Li and J. Liu, *Nano Lett.*, 2009, **9**, 800.
15 B. Yu, C. Liu, P.-X. Hou, Y. Tian, S. Li, B. Liu, F. Li, E. I. Kauppinen and H.-M. Cheng, *J. Am. Chem. Soc.*, 2011, **133**, 5232.
16 Y. Zhang, Y. Zhang, X. Xian, J. Zhang and Z. Liu, *J. Phys. Chem. B*, 2008, **112**, 3849.
17 P. Li and J. Zhang, *J. Mater. Chem.*, 2011, **21**, 11815.
18 G. Hong, B. Zhang, B. Peng, J. Zhang, W. M. Choi, J.-Y. Choi, J. M. Kim and Z. Liu, *J. Am. Chem. Soc.*, 2009, **131**, 14642-14643.
19 W. Zhou, S. Zhan, L. Ding and J. Liu, *J. Am. Chem. Soc.*, 2012, **134**, 14019.
20 X. Qin, F. Peng, F. Yang, X. He, H. Huang, D. Luo, J. Yang, S. Wang, H. Liu and L. Peng, and Y. Li, *Nano Lett*., 2014, **14**, 512.
21 L. Kang, Y. Hu, L. Liu, J. Wu, S. Zhang, Q. Zhao, F. Ding, Q. Li and J. Zhang, *Nano Lett*., 2014, **15**, 403.
22 Y. Chen, Y. Zhang, Y. Hu, L. Kang, S. Zhang, H. Xie, D. Liu, Q. Zhao, Q. Li and J. Zhang, *Adv. Mater.*, 2014, **26**, 5898.
23 M. Zheng, A. Jagota, E. D. Semke, B. A. Diner, R. S. McLean, S. R. Lustig, R. E. Richardson and N. G. Tassi, *Nat. Mater.*, 2003, **2**, 338.
24 R. Haddon, J. Sippel, A. Rinzler and F. Papadimitrakopoulos, *Mrs Bulletin*, 2004, **29**, 252.
25 G. S. Tulevski, A. D. Franklin, D. Frank, J. M. Lobez, Q. Cao, H. Park, A. Afzali, S.-J. Han, J. B. Hannon and W. Haensch, *ACS Nano*, 2014, **8**, 8730.
26 S. Salamat, X. Ho, J. Rogers and M. Alam, *Nanotechnology, IEEE Transactions on*, 2011, **10**, 439.
27 Y. Shibuta and S. Maruyama, *Chem. Phys. Lett.*, 2003, **382**, 381.
28 J.-Y. Raty, F. Gygi and G. Galli, *Phys. Rev. Lett.*, 2005, **95**, 096103.
29 C. L. Cheung, A. Kurtz, H. Park and C. M. Lieber, *J. Phys. Chem. B*, 2002, **106**, 2429.
30 Y. Li, R. Cui, L. Ding, Y. Liu, W. Zhou, Y. Zhang, Z. Jin, F. Peng and J. Liu, *Adv. Mater.*, 2010, **22**, 1508.
31 S. Hofmann, R. Sharma, C. Ducati, G. Du, C. Mattevi, C. Cepek, M. Cantoro, S. Pisana, A. Parvez and F. Cervantes-Sodi, *Nano Lett.*, 2007, **7**, 602.
32 F. Yang, X. Wang, D. Zhang, J. Yang, D. Luo, Z. Xu, J. Wei, J. Wang, Z. Xu and F. Peng, X. Li, R. Li, Y. Li, M. Li, X. Bai, F. Ding and Y. Li, *Nature*, 2014, **510**, 522.
33 H. Wang, Y. Yuan, L. Wei, K. Goh, D. Yu and Y. Chen, *Carbon*, 2015, **81**, 1.
34 X. Liang, J. Xiao, B. Chen and Y. Li, *Inorg. Chem.*, 2010, **49**, 8188.
35 N. Skorodumova, S. Simak, B. I. Lundqvist, I. Abrikosov and B. Johansson, *Phys. Rev. Lett.*, 2002, **89**, 166601.
36 C.-Y. Moon, Y.-S. Kim, E.-C. Lee, Y.-G. Jin and K. Chang, *Phys. Rev. B*, 2002, **65**, 155401.
37 B. Liu, W. Ren, S. Li, C. Liu and H.-M. Cheng, *Chem. Commun*., 2012, **48**, 2409.
38 P. T. Araujo, S. K. Doorn, S. Kilina, S. Tretiak, E. Einarsson, S. Maruyama, H. Chacham, M. A. Pimenta and A. Jorio, *Phys. Rev. Lett.*, 2007, **98**, 067401.
39 J. S. Soares, L. G. Cançado, E. B. Barros and A. Jorio, *Phys. Status Solidi B*, 2010, **247**, 2835.
40 M. S. Dresselhaus, G. Dresselhaus, R. Saito and A. Jorio, *Phys. Rep.*, 2005, **409**, 47.
41 Y. S. Lee, K. Y. Lim, Y. D. Chung, C. N. Whang and Y. Jeon, *Surf. Interface. Anal.*, 2000, **30**, 475.
42 S. Cheng-Min, H. Chao, Y. Tian-Zhong, X. Cong-Wen, E. Shu-Tang, D. Hao and G. Hong-Jun, *Chinese. Phys. Lett.*, 2008, **25**, 1479.
43 J. Li, C.-T. Ke, K. Liu, P. Li, S. Liang, G. Finkelstein, F. Wang and J. Liu, *ACS Nano*, 2014, **8**, 8564.